Two-dimensional interpretation of three-dimensional magnetotelluric data: an example of limitations and resolution

Juanjo Ledo,[1] Pilar Queralt,[2] Anna Martí[2] and Alan G. Jones[1]

[1]*Geological Survey of Canada,* 615 *Booth St.* K1A 0E9, *Ottawa, Ontario* K1A 0E9 *Canada.* E-mail: ledo@cg.nrcan.gc.ca
[2]*Departamento de Geodinàmica i Geofísica, Universitat de Barcelona, C/Martí i Franqués s/n. Barcelona 08028, Spain*

SUMMARY

Interpretation of magnetotelluric (MT) data for three-dimensional (3-D) regional conductivity structures remains uncommon, and two-dimensional (2-D) models are often considered an adequate approach. In this paper we examine 2-D interpretation of 3-D data by considering the synthetic responses of a 3-D structure chosen specifically to highlight the advantages and limitations of 2-D interpretation. 2-D models were obtained from inversion of the synthetic 3-D data set with different conditions (noise and distortion) applied to the data. We demonstrate the importance of understanding galvanic distortion of the data and show how 2-D inversion is improved when the regional data are corrected prior to modelling. When the 3-D conductive structure is located below the profile, the models obtained suggest that the effects of finite strike are not significant if the structure has a strike extent greater than about one-half of a skin depth. In this case the use of only TM-mode data determined better the horizontal extent of the 3-D anomaly. When the profiles are located away from the 3-D conductive structure the use of only TM-mode data can imagine phantom conductive structures below the profile, in this case the use of both polarizations produced a better determination of the subsurface structures. It is important to note that the main structures are identified in all the cases considered here, although in some cases the large data misfit would cause scepticism about features of the models.

Key words: electromagnetic induction, electromagnetic modelling, magnetotellurics, tensor decomposition.

INTRODUCTION

In recent years advances in computer technology have enabled the development of faster and more reliable algorithms to calculate the three-dimensional (3-D) electromagnetic response of earth models. Consequently, the current state-of-the-art for magnetotelluric (MT) data interpretation is that 3-D trial-and-error forward model fitting is being used more frequently for hypothesis testing, and 3-D inversions will become available in the near future. Data acquisition on dense 2-D grids has been undertaken to study geothermal (e.g. Takasugi *et al.* 1992) and mining-scale problems (e.g. Zhang *et al.* 1998), but regional-scale field experiments on a 2-D grid are often impractical due to high cost and inaccessibility. Accordingly, regional scale surveys are often restricted to a single profile or widely-separated profiles (e.g. southern British Columbia, Jones & Gough 1995; Ledo & Jones 2001). In such cases, researchers have to extract the maximum information possible from a data set that may be spatially undersampled. The use of additional geophysical information may allow 3-D modelling of MT data even where the data were collected along a profile (Pous *et al.* 1995; Park & Mackie 2000; Ledo *et al.* 2000).

Depending on the inductive and geological length scales of the target, 2-D interpretation of the data may be appropriate for a limited number of sites and over a limited period band. However, interpretation of 3-D data with 2-D techniques may not be able to reproduce the significant features of the subsurface; an example of this can be found in the 2-D interpretation of the Kayabe data set (Jones & Schultz 1997) by García *et al.* (1999).

In this paper, we explore some of the limitations of 2-D interpretation of 3-D MT data through the analysis of synthetic 3-D MT data with the currently available 2-D tools. Moreover, we demonstrate the importance of removing near-surface galvanic distortion on 3-D data, not only to reduce the error sources in a 2-D interpretation but also because of its importance in 3-D interpretation. Whilst this test is not aimed at reproducing all possible 3-D situations, we nevertheless follow procedures that we would undertake if these were actual field data to gain insight into the validity of 2-D modelling and interpretation of 3-D data.

SYNTHETIC DATA: 3-D MODEL

We have chosen a simple 3-D model to represent the regional structure for exploring the main problems arising from 2-D interpretation of 3-D data (Fig. 1). The model consists of a regional-scale 2-D dipping contrast beneath conductive overburden. We have embedded a 3-D elongated conductive body at an angle of −45 degrees with respect to the main 2-D structure. With this model, we can study two of the main problems associated with 2-D interpretation of 3-D data: the presence of structures with different strikes and the effects of finite body length. This model could represent a subhorizontal, kilometre-scale sill intrusion (i.e. mineralised layered intrusions such as the Bushveld or the Stillwater complex; Philpotts 1990) cross cutting at a medium angle an older 2-D regional structure. In another geological environment, Marquis *et al.* (1995) proposed
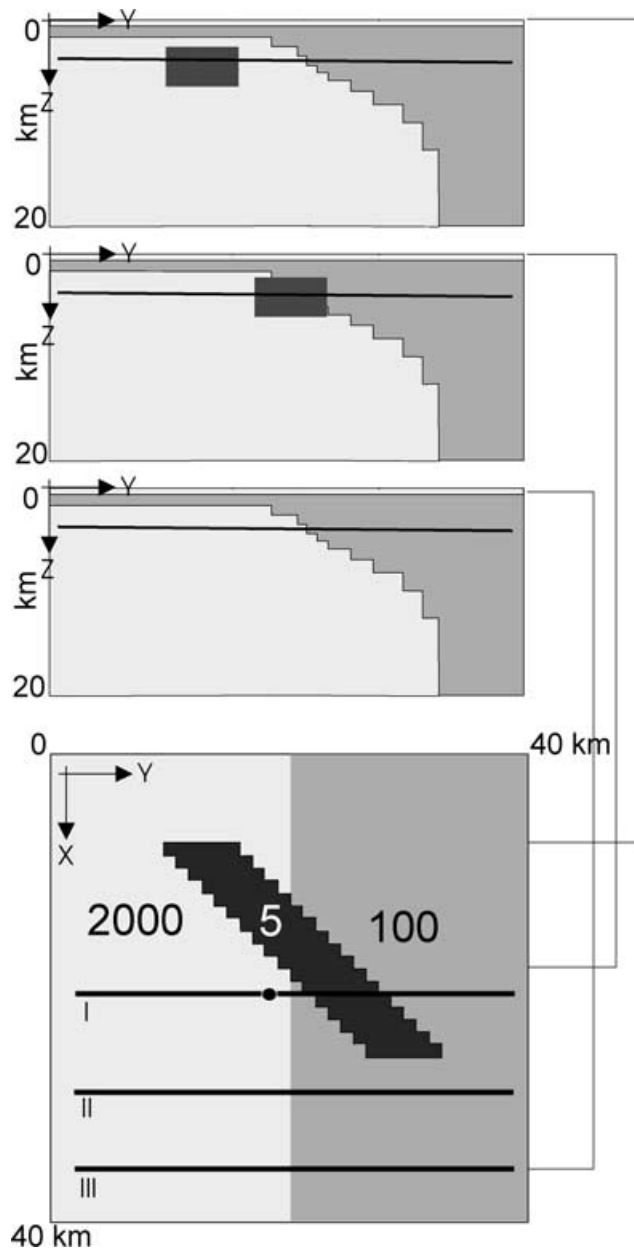
a strike-depth variation to explain the relationship between the allochtonous and autochtonous terranes across the boundary of the Intermontane and Omineca morphogeological belts in the Southern Canadian Cordillera.

The surface response of the 3-D model at 31 periods, between 0.01 and 1000 s, was calculated using the code of Mackie *et al.* (1994) with modifications by Mackie & Booker (2000, pers. comm.). To ensure reliability of the responses, the mesh was refined until convergence in the responses was obtained. The final mesh consisted of 99×99 horizontal elements and 50 vertical elements. Three profiles crossing the model were chosen, retrieving the data at every third node of the mesh for a total of 30 sites per profile. The data from profile I are influenced by the direction and finite strike of the 3-D conductive structure below it, whereas the data from profiles II and III are influenced by the nearby, off-profile presence of the 3-D conductive body.

In order to show the 3-D nature of the responses, we applied Groom–Bailey (G–B) decomposition (Groom & Bailey 1989) to the synthetic data from Profile I. Fig. 2 shows the unconstrained G–B galvanic distortion parameters twist and shear recovered from the data of profile I at four different periods with fixed strike direction (0°, along *x* direction on Fig. 1). Except at the shortest period (0.1 s), the values of these parameters are high, especially the shear. Given that there is no near-surface galvanic distortion affecting the data, these values describe the effects of the 3-D body. At short periods, between 0.1–10 s, the Groom–Bailey decomposition model is
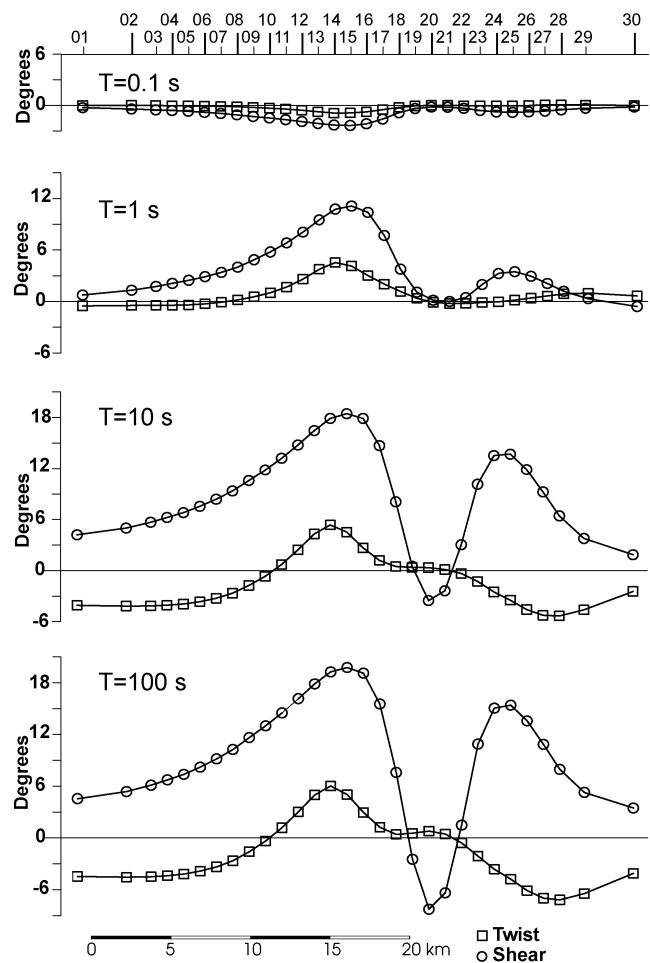

Figure 1. 3-D electrical conductivity regional model used in this work. Black lines on *xy* view indicate the position of the profiles. Black circle in Profile I: position of site 14.

Figure 2. Groom and Bailey parameters along the profile I used for four different periods. Circles: shear; squares: twist.
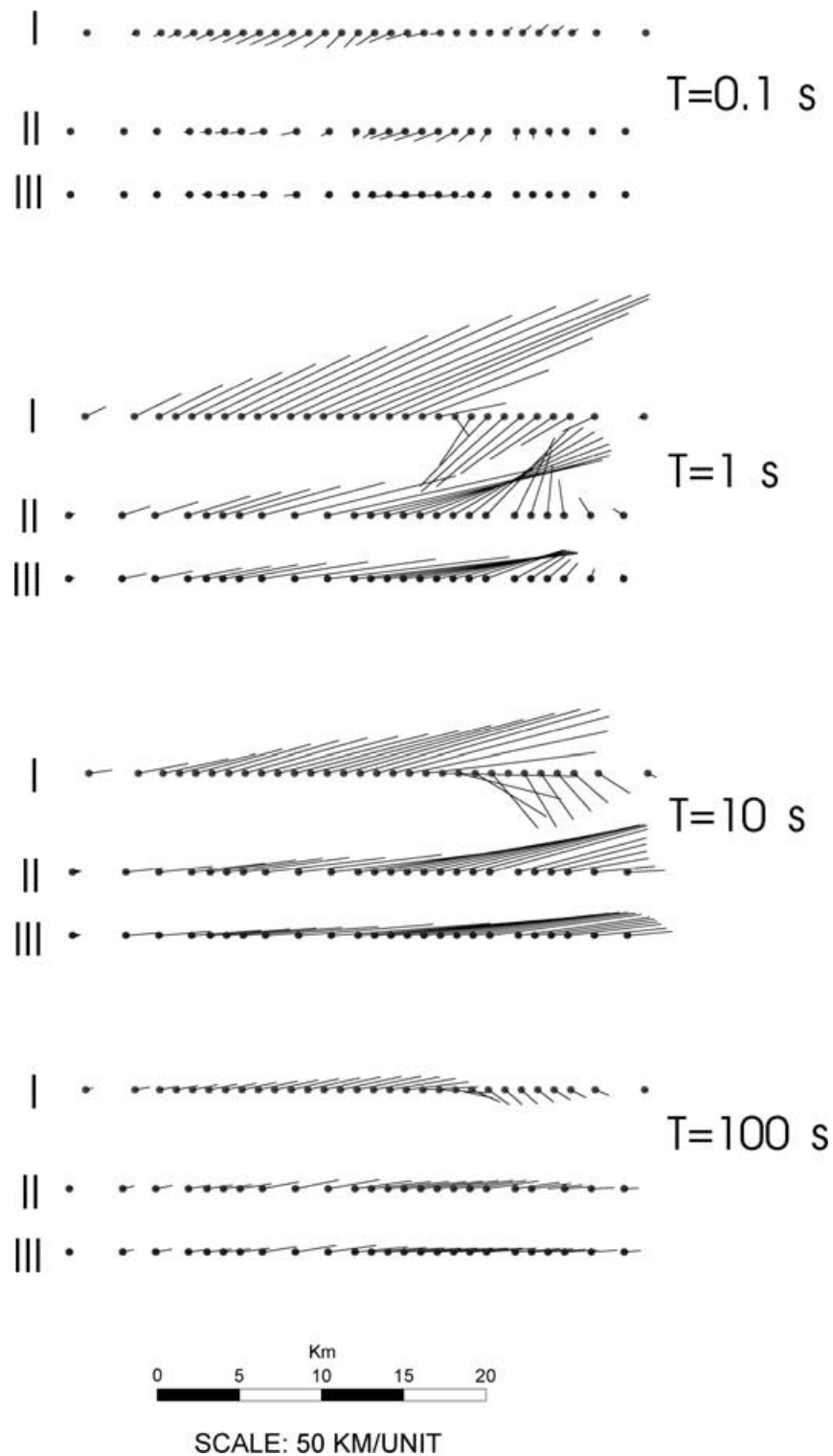
Figure 3. Real part of induction arrows (Parkinson's criterion) for the three profiles at four different periods.

inappropriate; the period dependence of the twists and shears indicates there are inductive effects associated with the 3-D body. At longer periods, 10 and 100 s, induction is weak and the response of the body can be validly described by a model which includes period independent galvanic effects. A more exhaustive analysis of the dimensionality of the data using the G–B technique will be presented below.

Fig. 3 shows the reversed real induction arrows following Parkinson's criteria (pointing towards current concentrations) for the three profiles at the same four periods discussed above. On profile I, the effect of the 3-D body alone can be observed for periods below 1 s, and at longer periods there is a combination of effects due to the 3-D body and the regional 2-D structure. On profiles II and III, induction arrows for periods of 1 s and 10 s
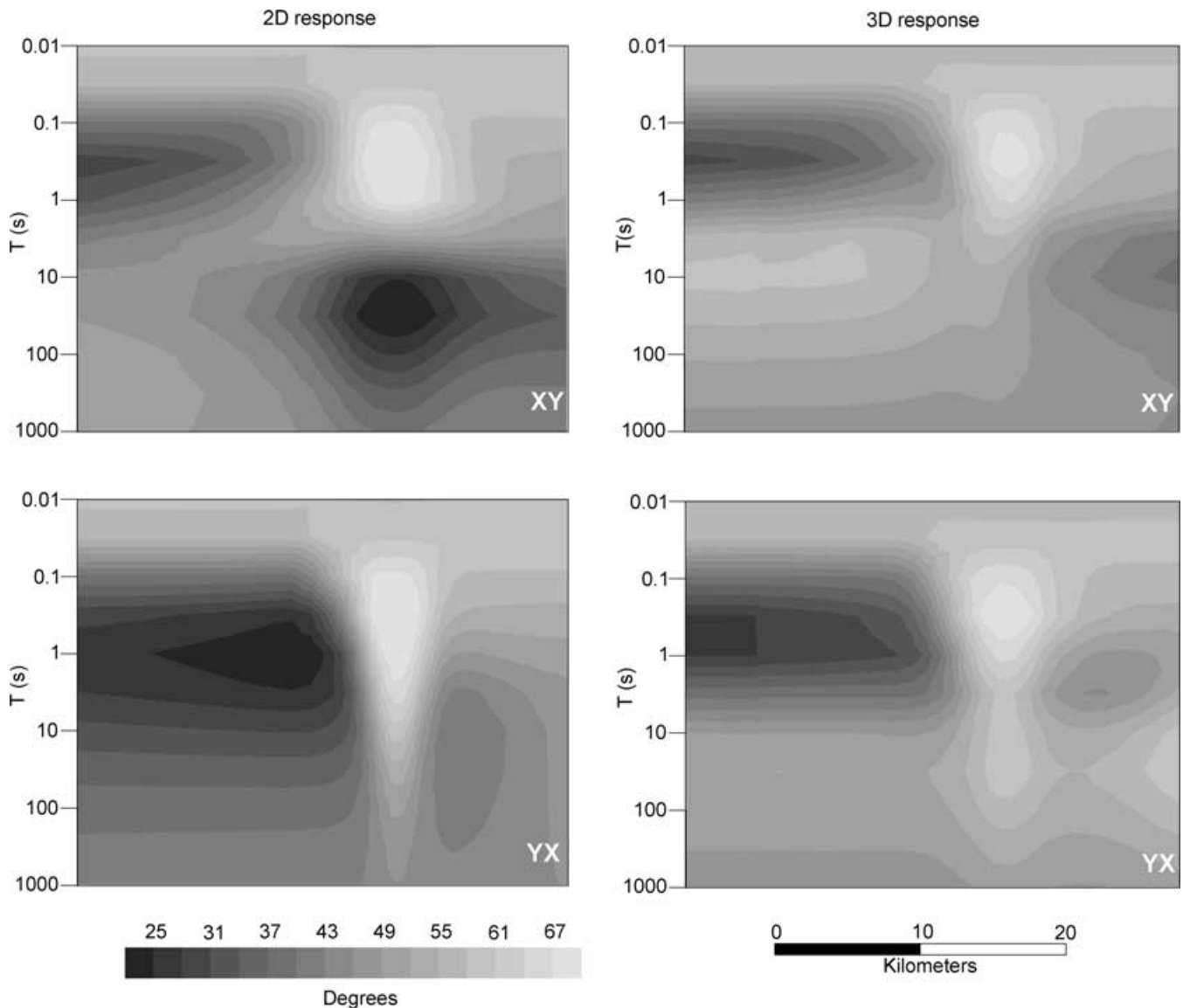
Figure 4. Comparison of the phases between the 3-D responses at Profile I and the response of the 2-D model (Fig. 9a) below Profile I.

are also strongly affected by the 3-D anomaly. Taken together the vertical magnetic fields and MT responses indicate that the model yields characteristics of a 3-D data set and facilitates our study of typical problems involved in 2-D interpretation of 3-D data.

Fig. 4 shows the phases obtained at profile I and the response of a 2-D model reproducing the structures below profile I. The difference between the responses of both models is readily apparent, reaching a maximum of $-22°$ in the centre of the profile.

3-D DATA AFFECTED BY GALVANIC DISTORTION

The near-surface galvanic distortions considered in this paper represent small-scale local scatterers over a regional structure (1-D, 2-D or 3-D). Following G–B, we can describe the effects by $\mathbf{Z} = \mathbf{C}\mathbf{Z}_R$,

where $\mathbf{Z}$ is the observed 2×2 complex impedance, $\mathbf{C}$ is a real 2×2 matrix period independent and $\mathbf{Z}_R$ is the 2×2 complex response of the regional structure.

To analyse the effects of near-surface galvanic distortion on regional 3-D responses, we applied galvanic distortions $\mathbf{C}$ to the synthetic impedance tensors from each site on profile I. The distortion matrices had the unresolvable static shift parameters (gain and anisotropy in G–B's description) set to unity, thus there are no unrecoverable amplitude scaling effects. Twist and shear parameters were assigned at random, (Fig. 5). To ensure distortion consistent with galvanic effects, period independent twists were bounded between $-60°$ and $60°$ and period independent shears between $-45°$ and $45°$, except for five sites where shears between $-60°$ and $60°$ were permitted. Fig. 6 shows the apparent resistivities and phases for site 14 on profile I before and after distortion was applied. In this case, the values of the twist and shear parameters were $40°$ and $5°$ respectively. For off-diagonal elements at short periods (Fig. 6a), the difference between
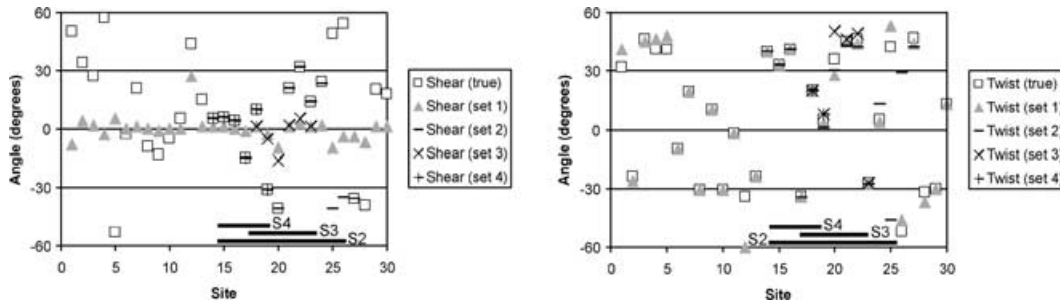
Figure 5. The strike directions obtained for each individual site of profile I. The arrows are scaled by the phase difference between the two off-diagonal elements. The maximum length of the arrows corresponds to a 20° difference. In (a) and (f) continuous thick lines represent the main boundaries present in the model.

them consists of only a period independent magnitude shift in the apparent resistivities (static shift, Jones 1988) and the phases are coincident. However, at periods longer than 0.1 s there is an important change in the shape of the curves because of the non-negligible values of the regional diagonal impedance tensor components. For the diagonal elements (Fig. 6b) the short period behaviour corresponds to 2-D in the principal direction (strike equal to 0°); the regional components are negligible and the distorted apparent resistivity curves are proportional to the regional ρ_{xy} and ρ_{yx} data.

In order to simulate real data being acquired along profile I, we added noise and scatter to the distorted response functions. The applied random scatter was around 1 per cent of the absolute value of the largest impedance at a particular period, and the associated error of that estimate was similarly varied. This process results in a data set with errors that varied in a random manner, rather than systematic, and was thereby more representative of field data.

TENSOR INVARIANTS AND BAHR'S CLASSIFICATION

The use of Mohr circles and magnetotelluric tensor invariants has been proposed by several authors for investigating the dimension-
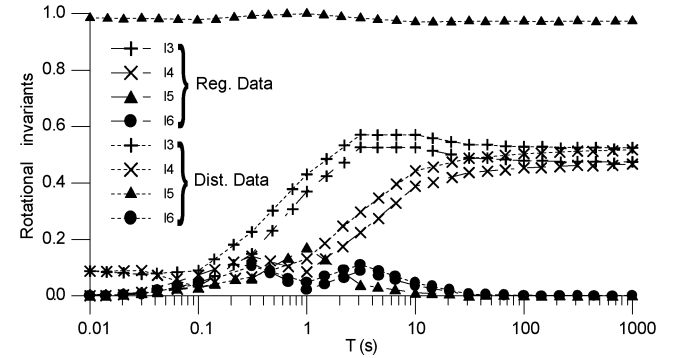

Figure 7. Apparent resistivities and phases for site 14; (a) off-diagonal components (b) diagonal components. Continuous line: regional data; discontinuous line: distorted data.

ality of magnetotelluric data (e.g. Lilley 1993; Szarka & Menvielle 1997; Weaver *et al.* 2000). Weaver *et al.* (2000) provide criteria for classifying the dimensionality and distortion based on the values of seven independent invariants, and we compared the invariants before and after recovering the regional data. Fig. 7 illustrates four
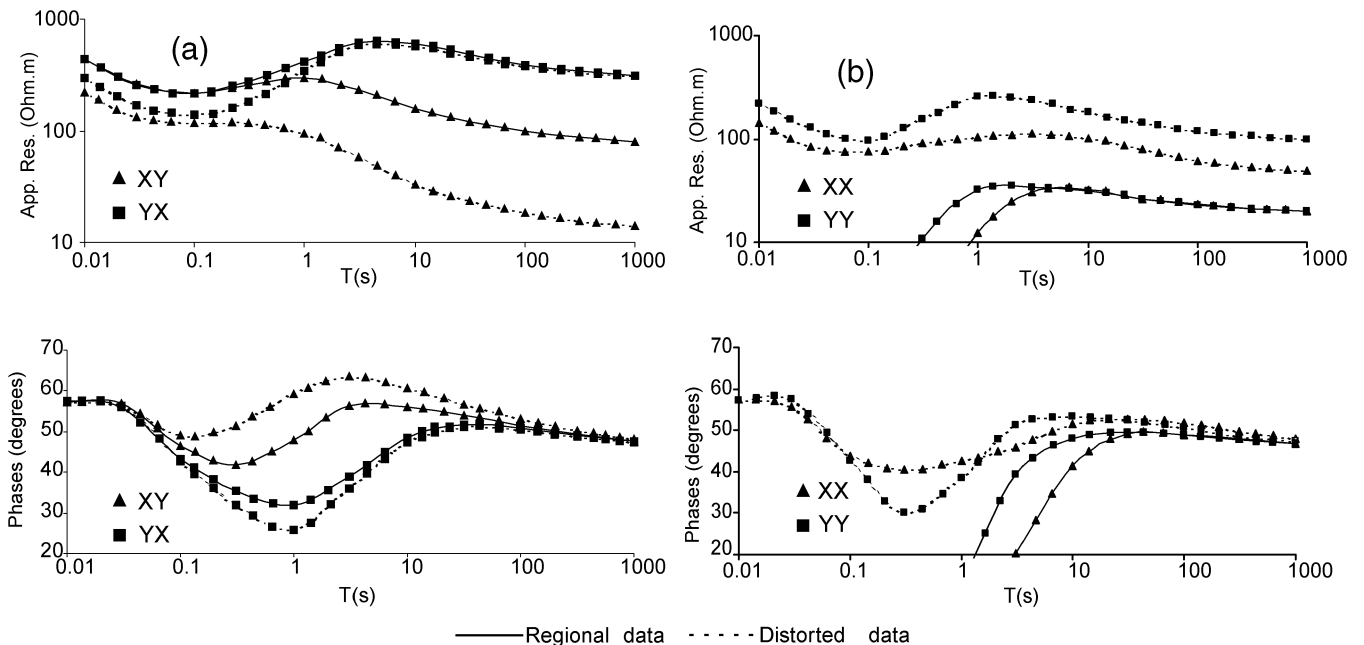

Figure 6. Groom and Bailey decomposition parameters obtained for all the distorted sites, site independent decomposition and multisite decomposition using different subset of sites. The sites used in each set are indicated by s2: set2, s3: set3 and s4: set4, see text for details.

Table 1. Classification of the impedance tensor dimensionality of site 014 (regional and distorted data) following Weaver *et al.*'s (2000) rotation invariants criteria.

Period (s)	Regional	Distorted
0.01	1-D	3-D/2-D $\theta = 4.5$
0.03	1-D	3-D
0.1	3-D	3-D
0.3	3-D	3-D
1	3-D/2-D $\theta = -25.9$	3-D/2-D $\theta = -25.9$
3	3-D	3-D
10	3-D	3-D
30	2-D $\theta = -21.6$	3-D/2-D $\theta = -21.6$
100	3-D	3-D
300	3-D	3-D
1000	3-D	3-D

of the invariants (I3, I4, I5 and I6) of the distorted and undistorted data for site 14. The other invariants (I1, I2 and I7) are not shown because there is no significant difference between the distorted and undistorted data, indicating that, for this model, they are related directly to the regional structure, whereas invariants I3, I4, I5 and I6 are affected by the distortion parameters. Using Weaver *et al.*'s (2000) classification criteria we have constructed Table 1 for the MT response for the different periods of the undistorted and distorted data. For the periods in which a 2-D regional structure is determined, the strikes are recovered and are listed in Table 1. From this invariant analysis, it is obvious that the data have a 3-D regional behaviour, but the analysis does not allow us to distinguish between 3-D effects caused by galvanic distortion and those caused by induction in 3-D structures.

Bahr (1991) published a classification scheme to describe galvanic distortion and regional conductivity structure aimed at aiding interpretation and Prácser & Szarka (1999) presented the correct

solution for some of Bahr's (1991) formulae. Using Bahr's scheme on the original and distorted, noisy synthetic data from site 014 we find the following:

(1) The skew value (κ) defined by Swift (1967) (Fig. 8a) is below 0.1 at all periods for the original 3-D data site and is greater than 0.8 for the distorted data at all periods. This important difference on the skew parameter between distorted and undistorted data had been pointed out previously by Chakridi *et al.* (1992). It is clear from the results obtained here that values of skew parameter below 0.1 can only be considered as a necessary, but not sufficient, condition for valid interpretation of an impedance tensor as 1-D.

(2) The rotationally invariant phase difference (μ) defined by Bahr (1991) is presented in Fig. 8(b). Small μ values are considered to be indicators of one-dimensionality. It is clear from the μ values obtained that the data cannot be considered 1-D and also that galvanic distortion affects the value of this parameter, given that in a 3-D environment the phases are affected by galvanic distortion independently of the rotation angle of the impedance tensor.

(3) The value of the rotationally invariant measure of two-dimensionality (Σ) is presented in Fig. 8(c). For periods >1 s this value is greater than 0.1 for both the distorted and undistorted data, and, following Bahr (1991), this is an indication of two-dimensionality of the long period data.

(4) Finally, the phase sensitive skew (η) defined by Bahr (1991) is shown in Fig. 8(d). A value greater than 0.3 was suggested by Bahr (1991) to be an indication of three-dimensionality. In our case, the value is smaller than 0.3 at all periods, for both the undistorted and distorted 3-D data.

Clearly, these parameters are highly dependent on the presence of local galvanic scatterrers. With the exception of the skew parameter the effects of the imposed galvanic distortions on Bahr's parameters are period dependent. These parameters appear to be useful to confirm a hypothesis about the dimensionality of the data, but not
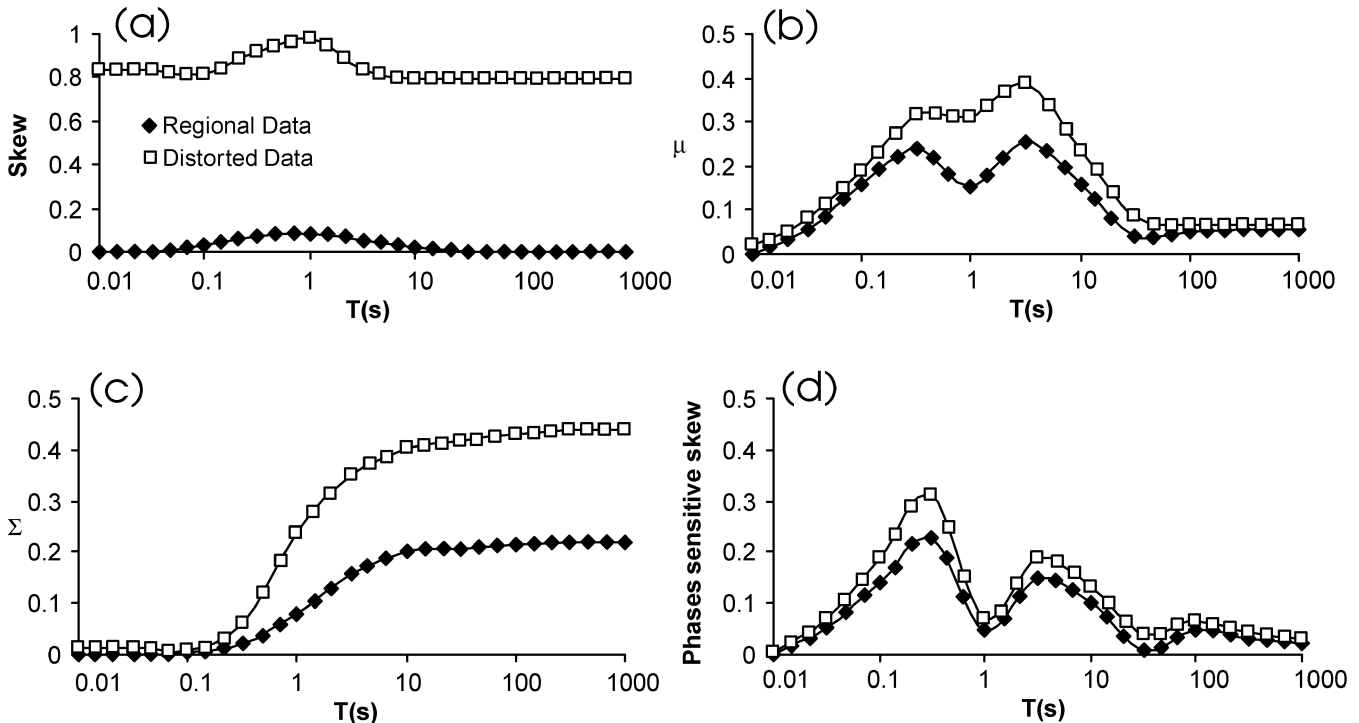

Figure 8. Weaver *et al.*'s (2000) invariants I3, I4, I5 and I6 for site 14. Dashed line, 3-D response; Dotted line, distorted data (see text for details).

2-D interpretation of 3-D MT data

to refute the hypothesis, i.e. if the phase sensitive skew, η, is greater than 0.3 the impedance tensor can be considered 3-D. The corollary does not hold: values of η below 0.3 do not necessarily imply that the impedance tensor is not 3-D.

In our opinion these parameters, as well as the tensor invariants, may be useful as a first approach to understand the behaviour of the data and to determine regional trends. Such analyses may be especially useful when dealing with large data sets. It must be borne in mind, however, that these methods lack error propagation to calculate the confidence limits, and that the threshold values suggested are not well justified by physical reasons.

2-D INVERSION OF 3-D DATA WITH GALVANIC DISTORTION

In this section we test the validity of 2-D interpretation of the noisy, distorted synthetic 3-D MT data from the stations along profile I. We apply different techniques to recover the regional data and subsequently invert them for structure. We follow three different procedures for handling the near-surface distortions. For the first case (Case A), we have adjusted the apparent resistivity curves to the same level as the undistorted data at short periods, to facilitate direct comparison with the other cases. Next, we considered that the regional data are 2-D affected by near-surface galvanic distortions and applied Groom-Bailey decomposition (Groom & Bailey 1989), (Case B). Finally, (Case C) we considered that the regional data are 3-D affected by near-surface galvanic distortions and applied the method of Ledo *et al.* (1998) to retrieve the regional 3-D responses.

For the different tests examined, we inverted the data using the algorithm of Rodi & Mackie (2001) assuming an error floor of 5 per cent for the apparent resistivities and 1.4° for phases. The starting model in all cases was a 100 $\Omega \cdot m$ half-space, and the iterative inversion ceased when the normalized rms misfit achieved was 1, or when the data misfit could not be improved. The *xy* data were assigned to the TE-mode (currents flowing along strike) and the *yx* data to the TM-mode (currents crossing structures; see *x* and *y* directions in Fig. 1). Fig. 9(a) shows the section (the vertical slice) of the 3-D model beneath the Profile I in Fig. 1.

To gain insight into the degree of resolution of the structures we can expect from the different cases we have calculated the 2-D response of model 8A and inverted the data. The inversion model obtained (Fig. 10) will help us to distinguish between structure due to 3-D effects or effects due to the inherent non-uniqueness of the inversion procedure.

Case A. The distorted apparent resistivities and phases for both modes (TE and TM) were inverted simultaneously. Only the distorted apparent resistivity curves are corrected at short periods to the same value as the undistorted curves for comparison purpose with the other cases. The model obtained after 37 iterations (Fig. 9b) has a global normalized rms misfit of 5.9, this is a poor fit of the data that is equivalent to an average misfit of 30 per cent in apparent resistivity and 8.3° in phase. To show how this 2-D model images the original structures, continuous lines overlying the model are drawn representing the boundaries of the main 3-D structures present directly below Profile I. The inversion model obtained shows the main subhorizontal contacts in the 3-D model. A conductive structure is also present; the lateral location of this structure and the top are well imaged, but the depth to the base of the conductive structure is overestimated. The fit to the TM data is reasonably good, but the TE comparison shows significant misfit at long periods. This misfit is illustrated in Fig. 11, which compares the distorted data

with the model response for site 14, taken as representative of the nature of the misfit along the whole profile. Although the inversion model seems to reproduce the main characteristics of the original structures, the poor fit of the model responses to the data would not lead us to have confidence in the inversion model obtained. The inversion of just the TM data produced the model show in Fig. 9(c); after 62 iterations the rms misfit achieved was 1.8. This model also shows the main subhorizontal contacts, and a conductive structure is again present; the lateral location of this structure and the top are well imaged, but the depth to the base of the conductive structure is underestimated.

Case B. For this second case, we have assumed that the data result from near surface galvanic distortion of the response of a regional 2-D structure. The data were analysed using the multisite, multi-period distortion decomposition code of McNeice & Jones (2001) (called M–J) which extends the approach first advocated by Bailey & Groom (1987), and subsequently Groom & Bailey (1989); Groom & Bailey (1991). Groom *et al.* (1993) and Jones & Dumas (1993) describe a step-by-step methodology for distortion decomposition analysis of a data set. McNeice & Jones (2001) extended this technique by permitting multiple sites and multiple periods to be analysed simultaneously to search for the most consistent distortion parameters and regional strike of the underlying 2-D structures. However, those authors cautioned strongly that the algorithm should not be used without scrutiny of the results obtained, as local minima can be found.

The procedure we have applied is as follows:

(1) The first step is to examine the data for systematic behaviour. Fig. 12 shows the period-dependent strike directions obtained for each individual site at six periods (0.1, 0.33, 1, 3, 10 and 100 s) using M–J tensor decomposition. The arrows are scaled by the phase differences between the two off-diagonal elements of the recovered regional 2-D impedance tensor and a 20° difference arrow is shown. This phase difference is a maximum in the regional strike direction, so the length of the arrows gives a visual measure of sensitivity to strike direction. Sites where the difference was smaller than 1°, or where the decomposition failed (as in the case where the applied shears were >45°), are not shown in Fig. 12. There is weak preferential strike direction at short periods (<0.1 s), i.e. the Earth appears 1-D at low periods, due to the phases being equal. The same happens at long periods (>100 s) for the western sites. For the central sites, there is a preference for a strike −45° to about 0.33–1 s, then a predominance of a strike direction of 0°.

These plots display similar behaviour to those obtained by Marquis *et al.* (1995) in the Southern Canadian Cordillera, who showed a 0.01–0.1 s short period strike of predominantly ∼N25°W, and a 0.1–100 s strike of ∼N20°E. The former was associated with the allochthonous terranes of the Canadian Cordillera, which are of up to 5–10 km in thickness extent. The longer period strike direction, representative of the bulk of the crust below ∼7 km, was interpreted as autochthonous North American basement rocks.

(2) To obtain the local distortion parameters, the short period data (<0.1 s) were analysed using four different sets of sites. The period band between 0.01–0.1 s was chosen based on the results obtained from the above decomposition analysis. The first set includes all the sites of the line, set 2 spans the 2-D regional structure and the 3-D anomaly (sites 014–027), set 3 consists of the six sites on top of the 3-D anomaly (sites 018–023), and set 4 consist of the sites 014–018. The results of M-J distortion decomposition are shown in Fig. 5, which compares the applied distortion parameters against
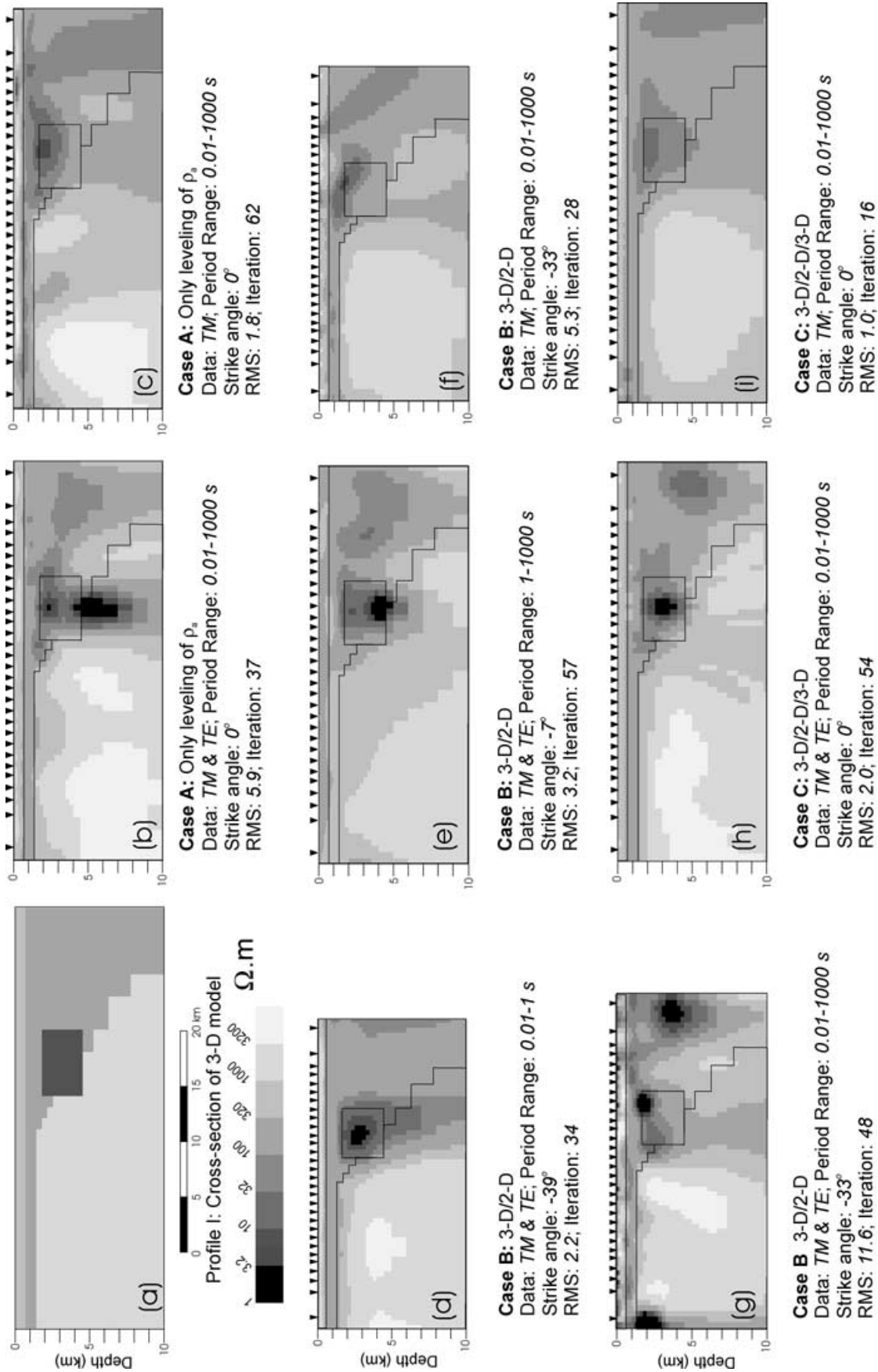
Figure 9. Bahr parameters for regional (black diamonds) and distorted (squares) data at site014. (a) Skew parameter; (b) μ parameter; (c) Σ parameter;(d) Phase sensitive skew (η) parameter.
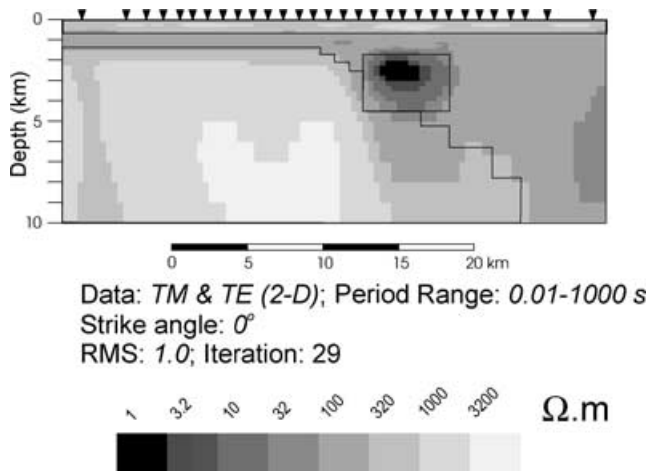
Figure 10. (a) the vertical slice of the 3-D model beneath the profile I (see Fig. 1). (b)–(i) different models obtained from different 2-D inversions (see text for details). Note that the models with strike not zero are smaller in horizontal extent due to the projection.
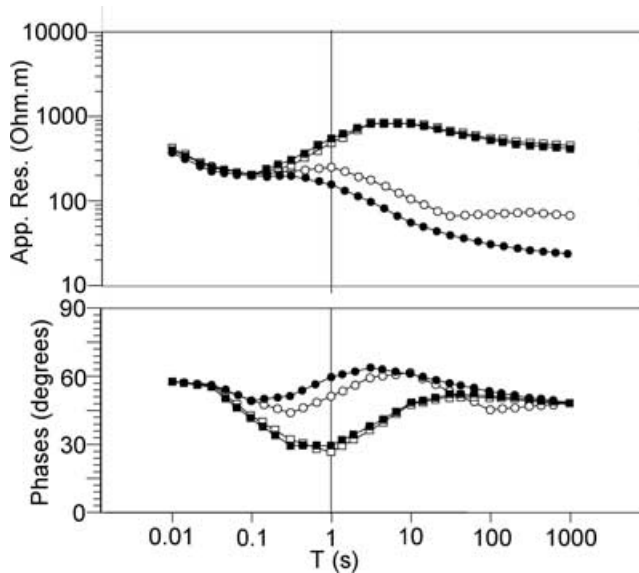

Figure 11. 2-D inversion model obtained from the inversion of the 2-D response of model 9a.

those derived. As discussed in Jones & Groom (1993) and McNeice & Jones (2001), twist is typically more stable than the other decomposition parameters, and such is also the case with these data. With the exception of those sites at which the applied distortions are inconsistent with the assumed model of distortion (shear values at sites 001, 004, 005, 025 and 026 exceed ±45°), and site 012 where the applied shear is close to 45°, the twists are well recovered. However, also evident is that one must carefully select the appropriate subset of data for distortion analysis. Using the whole line (set 1 in Fig. 5) resulted in shear estimates that are poorly determined; this results from including too many sites that do not sense the regional structure—which at these periods is the 3-D anomaly. Similarly, using only the sites on top of the anomaly (set 2 in Fig. 5) results in poor recovery of distortion parameters; penetration is attenuated by the presence of the anomaly and the data are not sensitive to its edges. The subset from over the resistive host to across the 3-D (set 3 in

Fig. 5) anomaly shows excellent recovery of both distortion parameters, except at the unphysical sites. The best results are obtained by choosing a subset (set 4 in Fig. 5) of sites that traverses over the two boundaries, sites 014–018. For this subset the distortion parameters are correctly recovered to within better than a degree in all cases.

Of course, without actual knowledge of the nature of the subsurface we would be challenged to know which of these analyses resulted in the most correct estimates. However, based on the sensitivity to strike direction of the responses shown in Fig. 5 we would choose subset 006–018 for analysis at short periods <1 s. The strike plots (Fig. 12) indicate that at short periods (<1 s) we can search for a consistent strike direction using sites 006–018 as representative of the uppermost crust. At the shortest periods, 0.01–0.033 s, there is no sensitivity to a preferred strike direction as the EM waves do not penetrate to the 3-D body. In the period band 0.033–1 s for sites 006–018, the best-fitting strike direction is −39°. At longer periods, >1 s, we would use data from the whole line, excluding those sites that do not fit the distortion model (sites 001, 004, 005, 025 and 026) to obtain the best-fitting average strike, and this is −7° for the period band 1–100 s.

On the basis of these results, and following the approach of Marquis *et al.* (1995), we consider two period ranges to undertake 2-D inversions for profile I. Upper crustal features, which respond in the short period band, 0.01–1 s, are assumed to have a 2-D strike of −39°. At long periods, 1–1000 s, the subsurface has an assumed strike of −7° and the data describe the deeper features; at these long periods the shallow 3-D structure is treated as galvanic distorter.

Fig. 9(d) shows the model obtained from inverting the recovered data between 0.01–1 s with a strike of −39°. The rms misfit of this model to the data is 2.15 and the inversion code reached convergence at iteration 34. Fig. 13 shows the comparison between the data and the model responses for site 14; the disagreement between the data and the model responses for both modes can only be observed in the phases for the highest period used. The model reproduces the location of the conductive structure and also the horizontal contacts. The model does not resolve the dipping contact between the 2000 Ω·m and 100 Ω·m structures below 6 km depth and the depth to the base of the conductive structure is overestimated. Both of these may be due to inadequate depth penetration at 1 s period.

From the long period decomposed regional data in the period band 1–1000 s, with strike fixed at −7°, we obtained the model shown in Fig. 9(e). This model fits the data to an rms misfit of 3.2 by iteration 57. Fig. 12 shows the comparison between the data and model responses for site 14; the TM-mode is acceptably fit, but the apparent resistivities of the TE-mode show some large misfit. The resolution of structures in the upper 2–3 km is poor due to the absence of short period data. However, the top of the conductive structure is imaged and its base is better determined than in the previous cases. The model also shows the dipping contact between the 2000 and 100 Ω·m structures in the eastern below 6 km depth. From the results obtained above the instinctive step might be to invert all the data, over the whole period range, but with varying strike. However, this step cannot be performed here, given not only the discontinuous response of the data for varying strike (see Fig. 13), but also because of the large difference of strike between the short and long period bands (32 degrees).

However, we have calculated the best strike angle for all sites taking into account all data between 0.01 and 1000 s. The best strike angle obtained from the M-J decomposition was of −33°. Figs 9(f) and (g) show the models obtained from the inversion of the recovered data for the TM data alone and for the TM and TE data respectively.
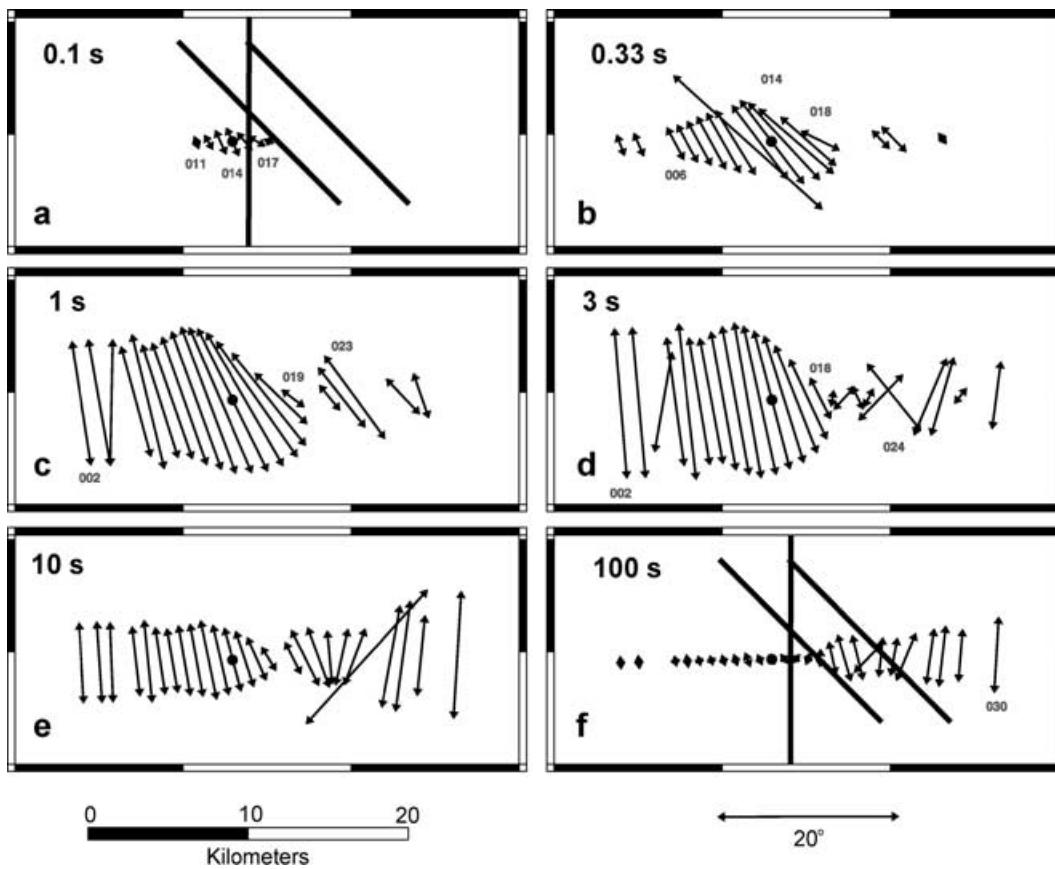
Figure 12. Comparison of apparent resistivities and phases for site 14 between the data from the 3-D model and the model response from case A (Fig. 9b). Black squares: 3-D TM-mode data; Black circles: 3-D TE-mode data; White squares: 2-D TM-response; White circles: 2-D TE-response.
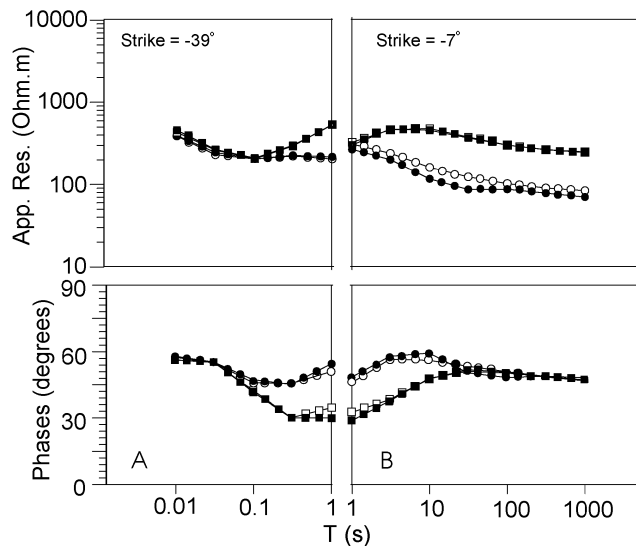

Figure 13. (a) Comparison of apparent resistivities and phases for site 14 between the Groom-Bailey corrected data from the 3-D model and the model response for T < 1 s (Fig. 9d). (b) Comparison of apparent resistivities and phases for site 14 between the Groom-Bailey corrected data from the 3-D model and the model response for T > 1 s (Fig. 9e). Black squares: 3-D TM-mode data; Black circles: 3-D TE-mode data; White squares: 2-D TM-response; White circles: 2-D TE-response.

These two models are not only the ones that present a larger rms misfit, but also the ones that present the highest disagreement with the true cross-section along Profile I.

Case C. Finally, we consider the data as 3-D affected by near surface galvanic distortions. Several approaches have been proposed recently to correct the data for 3-D near surface galvanic distortion of a 3-D regional subsurface, (i.e. Ledo *et al.* 1998; Utada & Munekane 2000; Garcia & Jones 2002). Here we applied the method proposed by Ledo *et al.* (1998) to retrieve the regional 3-D data that corresponds to a 3-D/2-D/3-D-superimposed model. This model consists of local, near-surface heterogeneities (3-D) over a 2-D regional structure for shallow depths (short periods), and a regional 3-D structure for greater depths (long periods). Given that galvanic distortion depends on the relationship between the local, near-surface heterogeneity and the surrounding media (Jiracek, 1990), the G–B decomposition method can be applied as usual to the short period data and, accordingly, the azimuthal strike, twist and shear parameters obtained and stripped off the responses over the whole period range, by simply resolving a linear set of equations (Ledo *et al.* 1998). Applying this method recovers the undistorted 3-D data.

After 54 iterations, the model obtained (Fig. 9) has an rms misfit of 2.0. From the comparison between the inversion model and the slice corresponding to the 3-D model, it is clear that the top of the conductive 3-D structure is well imaged, although the conductivity and the lateral boundaries are not well resolved. However, the top
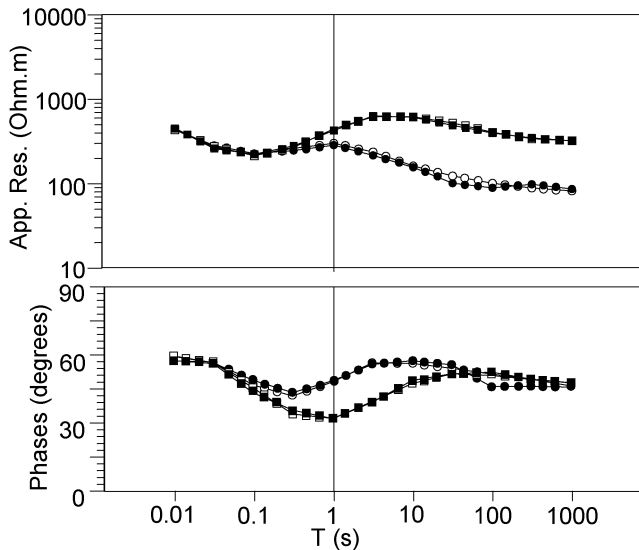
Figure 14. Comparison of apparent resistivities and phases for site 14 between data corrected following the scheme of Ledo *et al.* (1998) and from the model response (Fig. 9h). Black squares: 3-D TM-mode data; Black circles: 3-D TE-mode data; White squares: 2-D TM-response; White circles: 2-D TE-response.

layers and the main 2-D structure are well resolved. Fig. 14 shows the comparison between the data and the model responses for site 14. Obviously, this approach results in a better fit for both polarizations.

One approach to 3-D data interpretation is to invert the TM-mode data only, as they can be less affected by complex effects caused near the ends of 3-D structures (Wannamaker *et al.* 1984, and references therein). Such TM-mode only inversions have appeared extensively in the literature (e.g. Wannamaker *et al.* 1997; Wei *et al.* 2001), although questions have been raised about its general applicability (Park & Mackie 1997, 2000). Also, TM-mode data are insensitive to subvertical conductive structures (see, e.g. Vozoff 1972; Jones 1993). To test this approximation, we inverted the TM-mode data defined above in Case C. The model shown in Fig. 9(i) was obtained after 16 iterations and has an rms misfit of 1.0. The data fit is similar to that in Case C for the *yx* polarization data but the geometry of the 3-D structure is better resolved than in all previous cases, although its conductivity is underestimated. Consistent with previous work, this suggests that the model obtained using the *yx* data (TM-mode) is more robust than the one obtained using both polarizations. However, the dipping 2-D structure east of the conductive body is less visible than for case 9(i).

EFFECT OF 3-D STRUCTURES OUT OF THE PROFILE

We consider the effects of 3-D structures out of the profile by analysing the regional data (without distortion) from Profiles II and III (Fig. 1) which are not located over the conductive 3-D body. The inversion procedures were the same as for Profile I. As discussed in the section describing the 3-D model, the shorter period real induction arrows (Fig. 3) show that the responses from sites located close to the 3-D structure on Profile II are significantly affected by its presence. At longer periods, the regional 2-D structure controls the behaviour of the induction arrows. On Profile III the induction arrows are only marginally affected by the presence of the 3-D structure.

Profile II is 2 km distant from the edge of the 3-D structure, which is about half a skin depth at the period of maximum induction in the body (skin depth at ~1 s in a host of 100 $\Omega \cdot$ m is approximately 5 km). Inverting the data from both polarizations for the sites along this profile we achieve a final rms misfit of 1.6 after 70 iterations for the model illustrated in Fig. 15(a). The fit of the data is excellent for both polarizations. The continuous line overlying the model represents the boundary of the main structures present on the vertical slice below Profile II in Fig. 1 and the dashed line represents the projection of the end of the 3-D body into the plane of the profile. The main 2-D structure is recovered, with the dipping contact well defined to at least 5 km depth. There is an increase in conductivity coincident with the projection of the 3-D body due to 3-D effects. The inversion of the *yx*-polarization (TM-mode) data alone achieved an rms misfit of 1.0 after 25 iterations. The TM only model (Fig. 15b) also images the extension of the 3-D body, although it is not underneath the profile. This is surprising given that the edge of the body is half a skin depth away (see above), and currently accepted conviction is that the TM-mode data can be validly interpretable in a 2-D manner when the ends of the 3-D structures are more than 0.1 skin depths away (Jones 1983). However, the resistivity of the imaged phantom body is an order of magnitude higher than the true resistivity, so the approximation holds, albeit weakly. The 2-D regional structure is not as well resolved as when both polarizations are used (*cf.* Figs 15a and b). From the analysis of the induction arrows of Profile II (Fig. 3) it is clear that they are more affected by the 3-D conductive structure than are the MT impedance tensor components.

Profile III is located 7 km away from the edge of the 3-D body, which is 1.5 skin depths. The inversion of both polarizations after 31 iterations results in a model (Fig. 15c) with an rms misfit of 1.02. This model reproduces the main 2-D regional structure, and the 3-D body does not affect it, consistent with the ends of the structure being located more than a skin depth away (Jones 1983; Wannamaker *et al.* 1984). The inversion of the TM-mode data alone result in the model presented in Fig. 15(d) after 14 iterations with a final rms of 1.0. Again, using TM-mode data alone the regional 2-D structure is poorly imaged below 5 km depth.

DISCUSSION AND CONCLUSIONS

Synthetic data from a simple but illustrative model incorporating a 3-D conducting body of limited extent striking at 45° to a regional 2-D dipping structure provides a suitable data set to study typical problems associated with multidimensional magnetotelluric data interpretation. The analysis of induction arrows, rotational invariants, dimensionality indicators and Groom and Bailey distortion parameters can be useful tools to determine the appropriate dimensionality, but can be misleading if used without thought. Often a 2-D inversion is undertaken of data that exhibit weak 3-D effects because of the inadequacy of spatial coverage (only a single profile of data rather than a grid), because of the complexity of 3-D modelling, and because of the present inaccessibility of 3-D inversion codes. Thus, studies of the effects of finite strike of 3-D structures in a 2-D inversion are necessary to ascertain when a 2-D approximation may be valid.

Although the situations presented here are specific and are not aimed to reproduce all possible 3-D situations, they permit insight into the pitfalls of 2-D modelling and interpretation of 3-D data. One general conclusion we can draw from our study is the importance of removing local small-scale galvanic distortions prior to modelling the data, whether in 2-D or in 3-D. Models obtained from data
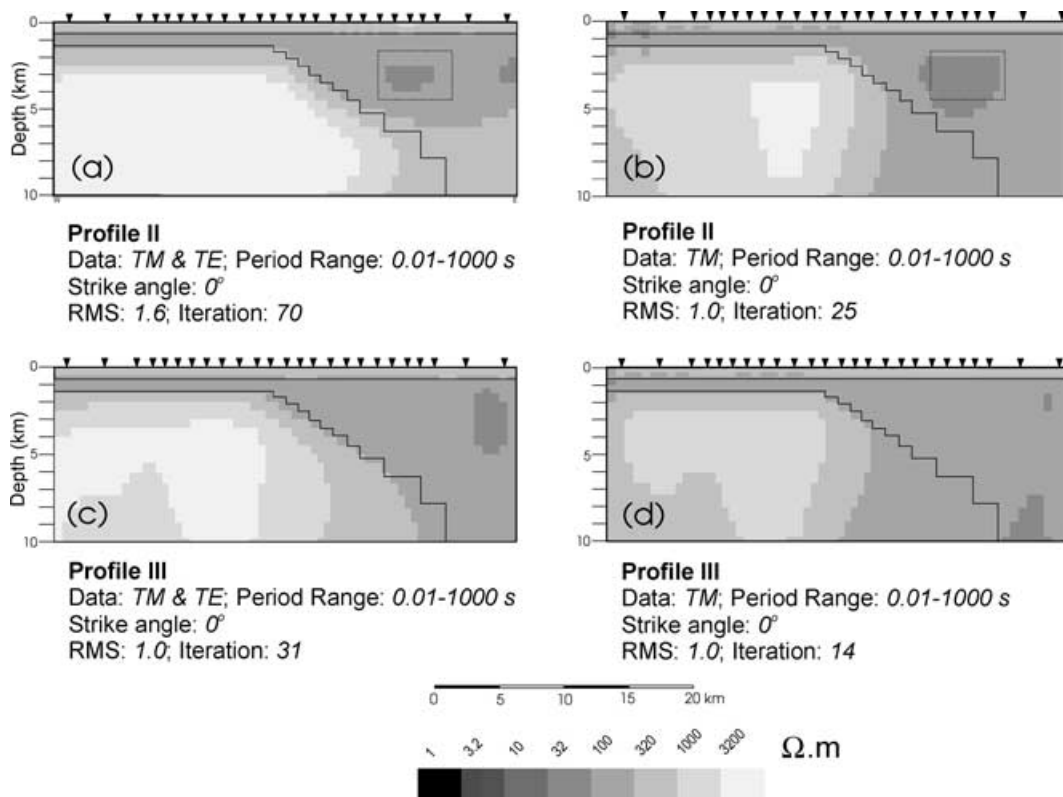
Figure 15. 2-D models obtained for profiles II and III, see text for details.

that have not had local distortions removed (Fig. 9b) poorly resolve structures compared to the models obtained from decomposed data (Figs 9c–j). The mixing of the regional diagonal and off-diagonal components produces a distortion that is period dependent and that also affects the phases in the 3-D case. Even for a high density grid of stations and efficient 3-D inversion codes there will always be the problem of spatial aliasing. We cannot model the Earth at all scales from the subelectrode array scale (metres) to the lithospheric scale (tens to hundreds of kilometres), so there may sometimes be a need for pre-processing the derived responses to remove the effects of small-scale scatterers.

From our examples we conclude that the effects of finite strike are not significant when the 3-D conductive structure is located below the profile and the structure has a strike extent greater than about one-half of a skin depth. Joint 2-D inversion of both the TE- and TM-mode responses resolved acceptably the top and location of the conductive structure. Inversion of TM-mode data only gave superior determination of the horizontal extent of the 3-D anomaly, although the deeper 2-D structures were not well imaged. However, when the profiles are located off the conductive 3-D body, TM-only 2-D inversion can image phantom conductive structures that are laterally off the profile. This phenomenon was also show by Wannamaker (1999). For our model, joint inversion of both modes reproduced the structures below the profile with more fidelity than the inversion of TM-only data. The rule-of-thumb of one host skin depth for joint 2-D inversion of both TE- and TM-mode data, advocated by Jones (1983) and Wannamaker *et al.* (1984), appears to hold. The interpretation of 3-D datasets with 2-D techniques seems to be valid if the length scale of the 3-D structures is higher than the inductive length scale.

Although we have shown the induction arrows to show the 3-D effects of the model used we did not include them during the

inversion procedure. Wannamaker (1999) showed that 3-D effects on a 2-D interpretation may produce different results when using the geomagnetic transfer functions, and this fact could be used as a consistency check.

Finally, it is important to note that all the inversion models obtained resemble the main characteristics of the true model. Thus, although the data are 3-D we obtained the first-order structures with 2-D techniques. Of course, in a real situation where the real model it is unknown, a sensitivity analysis of the main structures is required to determine which structures of the derived models are more credible.

REFERENCES

Bahr, K., 1991. Geological noise in magnetotelluric data: A classification of distortion types, *Phys. Earth planet. Inter.,* **66,** 24–38.

Bailey, R.C. & Groom, R.W., 1987. Decomposition of the magnetotelluric impedance tensor which is useful in the presence of channeling, *Exp. Abstr. 57th ann. Inter. S. exp. geophys., Tulsa,* **57,** 154–156.

Chakridi, R., Chouteau, M. & Mareschal, M., 1992. A simple technique for analysing and partly removing galvanic distortion from the magnetotelluric impedance tensor: Application to Abitibi and Kapuskasing data (Canada), *Geophys. J. Int.,* **108,** 917–929.

Garcia, X. & Jones, A.G., 2002. Extended decomposition of MT data, in, *Three-Dimensional Electromagnetics—II,* eds Zhdanov, M.S. & Wannamaker, P.E., Second International Gerald W. Hohmann Symposium, Elsevier, Amsterdam, in press.

Garca, X., Ledo, J. & Queralt, P., 1999. 2-D Inversion of 3-D magnetotelluric data: the Kayabe dataset, *Earth, Planets and Space,* **51,** 1135–1143.

Groom, R.W. & Bailey, R.C., 1989. Decomposition of the magnetotelluric impedance tensor in the presence of local three-dimensional galvanic distortion, *J. geophys. Res.,* **94,** 1913–1925.

Groom, R.W. & Bailey, R.C., 1991. Analytical investigations of the effects of near-surface three-dimensional galvanic scatterers on MT tensor decomposition, *Geophysics,* **56,** 496–518.

Groom, R.W., Kurtz, R.D., Jones, A.G. & Boerner, D.E., 1993. A quantitative methodology for determining the dimensionality of conductive structure from magnetotelluric data, *Geophys. J. Int.,* **115,** 1095–1118.

Jiracek, G., 1990. Near-surface and topographic distortions in electromagnetic induction, *Surv. Geophys.,* **11,** 163–203.

Jones, A.G., 1983. The problem of 'current channelling': a critical review, *Geophys. Surv.,* **6,** 79–122.

Jones, A.G., 1988. Static shift of magnetotelluric data and its removal in a sedimentary basin environment, *Geophysics,* **53,** 967–978.

Jones, A.G., 1993. The COPROD2 dataset: Tectonic setting, recorded MT data and comparison of models, *J. Geomag. Geoelectr.,* **45,** 933–955.

Jones, A.G. & Dumas, I., 1993. Electromagnetic images of a volcanic zone, *Phys. Earth planet. Inter.,* **81,** 289–314.

Jones, A.G. & Gough, D.I., 1995. Electromagnetic studies in southern and central Canadian Cordillera, *Can. J. Earth Sci.,* **3,** 1541–1563.

Jones, A.G. & Groom, R.W., 1993. Strike angle determination from the magnetotelluric tensor in the presence of noise and local distortion: rotate at your peril!, *Geophys. J. Int.,* **113,** 524–534.

Jones, A.G. & Schultz, A.S., 1997. Introduction to MT-DIW2 Special Issue, *J. Geomag. Geoelectr.,* **49,** 727–737.

Ledo, J.J. & Jones, A.G., 2001. Regional electrical conductivity structure of the southern Canadian Cordillera and its physical interpretation, *J. geophys. Res.,* **106,** 30 755–30 770.

Ledo, J.J., Queralt, P. & Pous, J., 1998. Effects of galvanic distortion on magnetotelluric data over a three dimensional structure, *Geophys. J. Int.,* **132,** 295–301.

Ledo, J.J, Ayala, C., Pous, J., Queralt, P., Marcuello, A. & Muñoz, J.A., 2000. New geophysical constraints on the deep structure of the Pyrenees, *Geophys. Res. Lett.,* **27,** 1037–1040.

Lilley, F.E.M., 1993. Magnetotelluric analysis using Mohr circles, *Geophysics,* **58,** 1498–1506.

Mackie, R.L., Smith, T.J. & Madden, T.R., 1994. Three-dimensional electromagnetic modeling using finite diferences equations: the magnetotelluric example, *Radio Sci.,* **29,** 923–935.

Marquis, G., Jones, A.G. & Hyndman, R.D., 1995. Coincident conductive and reflective lower crust across a thermal boundary in southern British Columbia, Canada, *Geophys. J. Int.,* **120,** 111–131.

McNeice, G.W. & Jones, A.G., 2001. Multisite, multifrequency tensor decomposition of magnetotelluric data, *Geophysics,* **66,** 158–173.

Park, S.K. & Mackie, R.L., 1997. Crustal structure at Nanga Parbat, northern Pakistan, from magnetotelluric soundings, *Geophys. Res. Lett.,* **24,** 2415–2418.

Park, S.K. & Mackie, R.L., 2000. Resistive (dry?) lower crust in an active orogen, Nanga Parbat, northern Pakistan, *Tectonophysics,* **316,** 359–380.

Philpotts, A.R., 1990. *Principles of Igneous and Metamorphic Petrology,* Prentice Hall, New Jersey.

Pous, J., Ayala, C., Ledo, J.J., Marcuello, A. & Sàbat, F., 1995. 3-D modelling of magnetotelluric and gravity data of Mallorca Island (Western Mediterranean), *Geophys. Res. Lett.,* **22,** 735–738.

Prácser, E. & Szarka, L., 1999. A correction to Bahr's 'phase deviation' method for tensor decomposition, *Earth, Planets and Space,* **51,** 1019–1022.

Rodi, W. & Mackie, R.L., 2001. Nonlinear conjugate gradients algorithm for 2-D magnetotelluric inversion, *Geophysics,* **66,** 174–187.

Swift, C.M., 1967. A magnetotelluric investigation of an electrical conductivity anomaly in the south-western United States, *PhD thesis,* Department of Geology and Geophysics, M.I.T., Cambridge, MA (reprinted in *Magnetotelluric Methods,* pp. 156–166, ed. Vozoff, K., Geophys. Reprint Ser. No. 5, 1988, SEG, Tulsa).

Szarka, L. & Menvielle, M., 1997. Analysis of rotational invariants of the magnetotelluric impedance tensor, *Geophys. J. Int.,* **129,** 133–142.

Takasugi, S., Tanaka, K., Kawakami, N. & Muramatsu, S., 1992. High spatial resolution of the resistivity structure revealed by a dense network MT measurements—A case study in the Minabikayabe area, Hokkaido, Japan, *J. Geomag. Geoelectr.,* **44,** 289–308.

Utada, H. & Munekane, H., 2000. On galvanic distortion of regional three-dimensional magnetotellurics impedances, *Geophys. J. Int.,* **140,** 385–398.

Vozoff, K., 1972. The magnetotelluric method in the exploration of sedimentary basins, *Geophysics,* **37,** 1, 98–141.

Wannamaker, P.E., 1999. Affordable magnetotellurics: Interpretation in natural environments, in *Three-Dimensional Electromagnetics,* eds Oristaglio, M. & Spies, B., Society of Exploration Geophysicists, Tulsa.

Wannamaker, P.E., Hohmann, G.W. & Ward, S.H., 1984. Magnetotelluric responses of three-dimensional bodies in layered earths, *Geophysics,* **49,** 1517–1533.

Wannamaker, P.E., Johnson, J.M., Stodt, J.A. & Booker, J.R., 1997. Anatomy of the southern Cordilleran hingeline, Utah and Nevada, from deep electrical resistivity profiling, *Geophysics,* **62,** 1069–1086.

Weaver, J.T., Agarwal, A.K. & Lilley, F.E.M., 2000. Characterization of the magnetotelluric tensor in terms of its invariants, *Geophys. J. Int.,* **141,** 321–336.

Wei, W. *et al.*, 2001. Detection of widespread fluids in the Tibetan crust by magnetotelluric studies, *Science,* **292,** 716–718.

Zhang, P., King, A. & Watts, D., 1998. Using magnetotellurics for mineral exploration, *SEG Annual Meeting Expanded Technical Program Abstracts with Biographies*, 68.